

A Framework for Cross-Layer Evaluation of 5G mmWave Cellular Networks in ns-3

Russell Ford, Menglei Zhang, Sourjya Dutta
 Marco Mezzavilla, Sundeep Rangan
 New York University
 Brooklyn, New York, USA
 {russell.ford,menglei,sdutta,
 mezzavilla,srangan}@nyu.edu

Michele Zorzi
 University of Padova
 Padova, Italy
 zorzi@ing.unife.it

ABSTRACT

The growing demand for ubiquitous mobile data services along with the scarcity of spectrum in the sub-6 GHz bands has given rise to the recent interest in developing wireless systems that can exploit the large amount of spectrum available in the millimeter wave (mmWave) frequency range. Due to its potential for multi-gigabit and ultra-low latency links, mmWave technology is expected to play a central role in 5th Generation (5G) cellular networks. Overcoming the poor radio propagation and sensitivity to blockages at higher frequencies presents major challenges, which is why much of the current research is focused at the physical layer. However, innovations will be required at all layers of the protocol stack to effectively utilize the large air link capacity and provide the end-to-end performance required by future networks.

Discrete-event network simulation is a useful tool for researchers and will no doubt be invaluable for evaluating novel 5G protocols and systems from an end-to-end perspective. In this work, we present the first-of-its-kind, open-source framework for modeling mmWave cellular networks in the ns-3 simulator. Channel models are provided along with a configurable physical and MAC-layer implementation, which can be interfaced with the higher-layer protocols and core network model from the ns-3 LTE module for simulating end-to-end connectivity. The framework is demonstrated through several example simulations showing the performance of our custom mmWave stack.

Categories and Subject Descriptors

I.6.5 [Simulation and Modeling]: Model Development—*Modeling methodologies*; I.6.7 [Simulation and Modeling]: Simulation Support Systems—*Environments*

General Terms

Simulation; Modeling; Architecture; Design; Performance; Cellular; Wireless.

Keywords

mmWave; 5G; Cellular; Channel; Propagation; PHY; MAC.

1. INTRODUCTION

Millimeter Wave (mmWave) communications promises to be highly disruptive for both cellular and wireless LAN technology due to the potential for multi-gigabit wireless links, which make use of the gigahertz of contiguous bandwidth available at mmWave frequencies in combination with high-dimension antenna arrays for high-gain directional transmission. Although the mmWave channel is known to suffer from poor high-frequency propagation loss, advances in physical layer technology such as adaptive smart antennas along with recent work on channel measurements and modeling have paved the way for achieving sufficient range and coverage in these networks [1, 2]. Nevertheless, before mmWave technology can be effectively realized in 5G cellular networks, there are numerous challenges to be addressed not only at the physical layer but at higher layers of the radio stack and in the core network, as well. For instance, the extreme susceptibility of mmWave links to shadowing from blockages will require frequent, near instantaneous handover between neighboring cells, fast link adaptation, and a TCP congestion control algorithm that can utilize the large capacity when available but adapt quickly to rapid channel fluctuations to avoid congestion. Therefore, the constraints and characteristics of the mmWave physical layer will require novel solutions throughout the network and across all layers of the stack.

Discrete-event network simulators have, for long, been one of the most powerful tools available to researchers for developing new protocols and simulating complex networks. The ns-3 network simulator [3] currently implements a wide range of protocols in C++, making it particularly useful for cross-layer design and analysis.

In this work, we present the first millimeter wave module for ns-3, which can be used to evaluate cross-layer and end-to-end performance of 5G mmWave networks. We discuss the current state of the module, including a number of enhancements and added features since it was first introduced in [4], such as an improved statistical channel model based on 28 GHz channel measurements as well as a new ray tracing model. Custom implementations of a “LTE-like” Physical (PHY) and Medium Access Control (MAC) layer are also provided, which are based on the ns-3 LTE LENA module [5] architecture, and can easily be interfaced with the LENA

radio stack and core network. The PHY and MAC classes are parameterized and highly customizable in order to be flexible enough for testing different designs and numerologies without major modifications to the source code.

The rest of the paper is organized as follows. In Section 2, we introduce the overall architecture of the mmWave module framework. We then take a closer look at each component, starting with the PHY layer and channel models in Sections 3. Section 4 follows with a discussion on the MAC layer, which includes several scheduler classes as well as support for Adaptive Modulation and Coding (AMC) and Hybrid Automatic Repeat Request (HARQ). In Section 5, to demonstrate how the framework can be used for cross-layer evaluation, we provide some example simulations showing (i) the capacity of a TDMA mmWave cell with multiple users and (ii) the performance of TCP for single-user under varying channel conditions. Finally, we discuss future work and conclude the paper in Section 6.

2. MMWAVE FRAMEWORK OVERVIEW

Presently, the ns-3 mmWave module is targeted for simulating LTE-style cellular networks and is based heavily on the architecture and design patterns of the LTE LENA module. This enables the mmWave classes to interface with the higher-layer stack from LENA in order to leverage the robust suite of LTE/EPC protocols it provides.

In Figure 1, we see the high-level composition of the `MmWaveEnbNetDevice` and `MmWaveUeNetDevice` classes, which respectively represent the mmWave eNodeB (eNB) base station and User Equipment (UE) radio stacks. A more detailed UML class diagram is given in Figure 1 of [4] and details on each layer will be given in their respective sections. The `MmWaveEnbMac` and `MmWaveUeMac` MAC layer classes implement the LTE module Service Access Point (SAP) *provider* and *user* interfaces, which allow them to interoperate with the LTE Radio Link Control (RLC) layer. Support for RLC Saturation Mode (SM), Unacknowledged Mode (UM) and Acknowledged Mode (AM) is built into the MAC and scheduler classes (i.e. `MmWaveMacScheduler` and derived classes). The MAC scheduler also implements a SAP for configuration by the LTE RRC layer (`LteEnbRrc`). Therefore, all the components required for Evolved Packet Core (EPC) connectivity are available.

The `MmWavePhy` classes handle directional transmission and reception of the DL and UL data and control channels based on control messages from the MAC layer. Similar to the LTE module, each PHY instance communicates over the channel (i.e. `SpectrumChannel`) via an instance of the `MmWaveSpectrumPhy` class, which is shared for both the DL and UL (instead of separate such objects like in LTE LENA). Instances of `MmWaveSpectrumPhy` encapsulate all PHY-layer models including those for interference calculation (`MmWaveInterference`), Signal to Interference and Noise Ratio (SINR) calculation (`MmWaveSinrChunkProcessor`), the Mutual Information (MI)-based error model (`MmWaveMiErrorModel`), which computes packet error probability, as well as the Hybrid ARQ PHY-layer entity (`MmWaveHarqPhy`) for performing soft combining.

A more detailed exposition of the procedures and interactions of these classes is given in [4]. Since the structure, high-level functions and naming scheme of each class closely follows the LTE LENA module, the reader is also referred

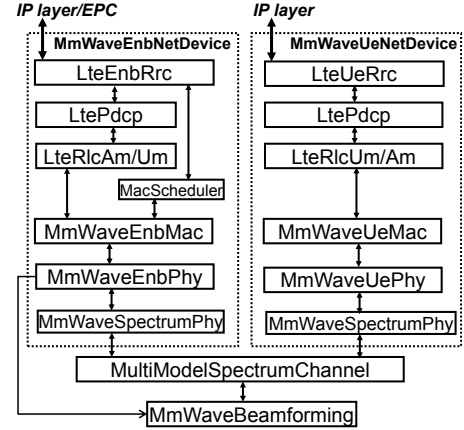


Figure 1: Simplified class diagram for the mmWave module.

to the LENA project documentation for more information [5].

3. PHYSICAL LAYER

In this section, we discuss the key features of the mmWave PHY layer. Specifically, we have implemented a TDD frame and subframe structure, which has similarities to TD-LTE, but allows for more flexible allocation and placement of control and data channels within the subframe and is suitable for the *variable Transmission Time Interval (TTI)* MAC scheme described in Section 4. Significant improvements have also been made to the channel model since the version introduced in [4]; The 28 GHz statistical path loss model can now be combined with the *building obstacle* model to simulate a realistic shadowing environment. A ray tracing-based path loss and fading model, which makes use of paths generated from measurements or by third-party ray tracing software, has also been added. Additionally, we have modified the LENA error model and Hybrid ARQ model to be compatible with our custom mmWave PHY and numerology (for instance, to support larger TB and codeword sizes as well as multi-process stop-and-wait HARQ for both DL and UL).

3.1 Frame Structure

It is widely contended that 5G mmWave systems will target Time Division Duplex (TDD) operation because it offers improved utilization of wider bandwidths and the opportunity to take advantage of channel reciprocity for channel estimation [1, 6, 7]. In addition, shorter symbol periods and/or slot lengths have been proposed in order to reduce radio link latency [8, 9]. The ns-3 mmWave module therefore implements a TDD frame structure which is designed to be configurable and supports short slots in the hope that it will be useful for evaluating different potential designs and numerologies. These parameters, shown in Table 1, are accessible through the common `MmWavePhyMacCommon` class, which stores all user-defined configuration parameters used by the PHY and MAC classes.

The frame and subframe structures share some similarities with LTE in that each frame is subdivided into a number of subframes of fixed length. However, in this case, the user is

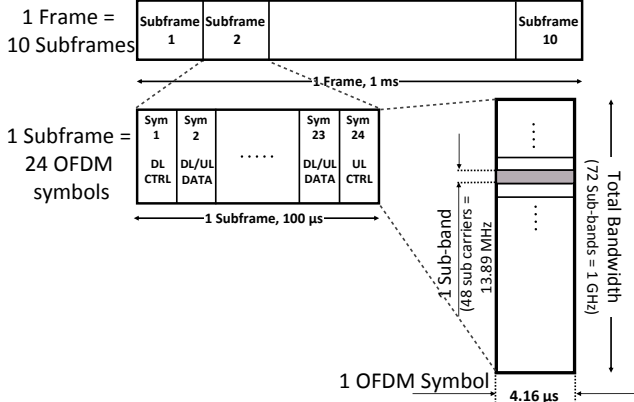


Figure 2: Proposed mmWave frame structure.

allowed to specify the subframe length in multiples of Orthogonal Frequency-Division Multiplexing (OFDM) symbols.¹ Within each subframe, a variable number of symbols can be assigned by the MAC scheduler and designated for either control or data channel transmission. The MAC entity therefore has full control over multiplexing of physical channels within the subframe, as discussed in Section 4. Furthermore, each variable-length time-domain data slot can be allocated by the scheduler to different users for either the uplink (UL) or downlink (DL).

Figure 2 shows an example of the frame structure with the numerology taken from our proposed design in [9]. Each frame of length 1 ms is split in time into 10 subframes, each of duration 100 μ s, representing 24 symbols of approximately 4.16 μ s in length. In this particular scheme, the downlink and uplink control channels are always fixed in the first and last symbol, respectively, of the subframe. A switching guard period of one symbol period is introduced each time the direction changes from UL to DL. In the frequency domain, the entire bandwidth of 1 GHz is divided into 72 sub-bands of width 13.89 MHz, each of which is composed of 48 sub-carriers. It is possible to assign UE data to each of these sub-bands, as is done with Orthogonal Frequency-Division Multiple Access (OFDMA) in LTE, however only TDMA operation is currently supported for reasons we shall explain shortly.

3.2 PHY Transmission and Reception

The `MmWaveEnbPhy` and the `MmWaveUePhy` classes model the physical layer for the mmWave eNodeB and the UE, respectively, and encapsulate similar functionality to the `LtePhy` classes from the LTE module. Broadly, these objects (i) handle the transmission and reception of physical control and data channels (analogous to the PDCCH/PUCCH and PDSCH/PUSCH channels of LTE), (ii) simulate the start and the end of frames, subframes and slots and (iii) deliver received and successfully decoded data and control packets to the MAC layer.

¹Though a many waveforms are being considered for 5G systems, OFDM is still viewed as a possible candidate. Therefore, we naturally choose to adopt OFDM, at least initially, for the mmWave module, which allows us to leverage the existing PHY models derived for OFDM from the LTE LENA module.

In `MmWaveEnbPhy/MmWaveUePhy`, calls to `StartSubFrame()` and `EndSubFrame()` are scheduled at fixed periods, based on the user-specified subframe length, to mark start and the end of each subframe. The timing of variable-TTI slots, controlled by scheduling the `StartSlot()` and `EndSlot()` methods, is dynamically configured by the MAC via the MAC-PHY SAP method `SetSfAllocInfo()`, which enqueues a `SfAllocInfo` allocation element for some future subframe index specified by the MAC. A *subframe indication* to the MAC layer triggers the scheduler at the beginning of each subframe to allocate a future subframe. For the UE PHY, `SfAllocInfo` objects are populated after reception of Downlink Control Information (DCI) messages. At the beginning of each subframe, the current subframe allocation scheme is dequeued, which contains a variable number of `SlotAllocInfo` objects. These, in turn, specify contiguous ranges of OFDM symbol indices occupied by a given slot, along with the designation as either DL or UL and control (*CTRL*) or data (*DATA*).

The data packets and the control messages generated by the MAC are mapped to a specific subframe and slot index in the *packet burst map* and *control message map*, respectively. Presently, in our custom subframe design, certain control messages which must be decoded by all UEs such as the DCIs are always transmitted in fixed PDCCH/PUCCH symbols at the first and last symbol of the subframe, but this static mapping can easily be changed by the user.² Other UE-specific control and data packets are recalled at the beginning of each allocated TDMA data slot and are transmitted to the intended device.

To initiate transmission of a data slot, the eNB PHY first calls `AntennaArrayModel::ChangeBeamformingVector()` to update the transmit and receive beamforming vectors for both the eNB and UE. In the case of control slots, no beamforming update is applied since we currently assume an “ideal” control channel. For both DL and UL, either the `MmWaveSpectrumPhy` method `StartTxDataFrame()` or `StartTxCtrlFrame()` is then called to transmit a data or control slot, respectively. The functions of `MmWaveSpectrumPhy`, which are similar to the corresponding LENA class, are as follows. After the reception of data packets, the PHY layer calculates the SINR of the received signal in each sub-band, taking into account the path loss, MIMO beamforming gains and frequency-selective fading. This triggers the generation of Channel Quality Indication (CQI) reports, which are fed back to the base station in either UL data or control slots. The error model instance is also called to probabilistically compute whether a packet should be dropped by the receiver based on the SINR and, in the case of a HARQ retransmission, any soft bits that have been accumulated in the PHY HARQ entity (see Section 4.3). Uncorrupted packets are then received by the `MmWavePhy` instance, which forwards them up to the MAC layer SAP.

3.3 Channel Models

The mmWave module allows the user to choose between two channel models. The first, implemented in the `MmWave-`

²Like in [8, 9], we assume either FDMA or SDMA-based multiple access in the control regions. However, we do not currently model these modulation schemes nor the specific control channel resource mapping explicitly. We intend for this capability to be available in later versions, which will enable more accurate simulation of the control overhead.

Parameter Name	Default Value	Description
<i>SubframePerFrame</i>	10	Number of subframes in one frame
<i>SubframeLength</i>	100 μ s	Length of one subframe in μ s
<i>SymbolsPerSubframe</i>	24	Number of OFDM symbols per slot
<i>SymbolLength</i>	4.16 μ s	Length of one OFDM symbol in μ s
<i>NumSubbands</i>	72	Number of sub-bands
<i>SubbandWidth</i>	13.89e6	The width of one sub-band in Hz
<i>SubcarriersPerSubband</i>	48	Number of subcarriers in each sub-band
<i>CenterFreq</i>	28e9	The carrier frequency in Hz
<i>NumRefScPerSymbol</i>	864 (25% total)	Reference subcarriers per symbol
<i>NumDlCtrlSymbols</i>	1	Downlink control symbols per subframe
<i>NumUlCtrlSymbols</i>	1	Uplink control symbols per subframe
<i>GuardPeriod</i>	4.16 μ s	Guard period for UL-to-DL mode switching
<i>MacPhyDataLatency</i>	2	Subframes between MAC scheduling request and scheduled subframe
<i>PhyMacDataLatency</i>	2	Subframes between TB reception at PHY and delivery to MAC
<i>NumHarqProcesses</i>	20	Number of HARQ processes for both DL and UL

Table 1: Parameters for configuring the mmWave PHY.

PropagationLossModel and **MmWaveBeamforming** classes, is based off our previous code in [4], which is derived from extensive MATLAB[®] simulation of the 28 GHz channel presented in [2]. This model has now been combined with the built-in **BuildingsObstaclePropagationLossModel** for simulating mobility. The second model, the **MmWaveChannel-Raytracing** class, uses data obtained from measurements or third-party ray tracing software such as WinProp [10]. The details each model are as follows.

3.3.1 Simulation-Generated Statistical Model

A full discussion on the simulation based channel model is available in [4]. We have strengthened this model by incorporating a building obstacle propagation model which enables simulation of UE mobility through a shadowing environment. For each simulation, instances of the building class (built into ns-3) are used to simulate obstacles. The channel state is updated based on the relative position of the transmitter, receiver and the buildings as the UE moves through the environment. A virtual line is drawn between the transmitter and receiver. If this line intersects any building we assign the channel state as NLoS; Otherwise, we assign a LoS channel.

After selecting the channel state, the propagation loss can be computed as

$$PL(d)[dB] = \alpha + \beta 10 \log_{10}(d) + \xi, \quad \xi \sim N(0, \sigma^2), \quad (1)$$

where ξ represent shadowing, parameter d is the distance from receiver to transmitter and the values of parameter α , β , and σ for each channel state are given in [2]. In this model, we consider the channel to be in outage if the distance between the transmitter and the receiver exceeds a predefined threshold.

Due to lack of information about diffraction effects in mmWave channel, we assume the propagation loss increases or decreases suddenly without a transition period when the channel state changes. We hope to model diffraction more accurately in our future work.

Channel matrix. Following the method in [2], to compute the long-term statistical characterization of the mmWave channel, we model the mmWave channel as a combination of clusters, each composed of several subpaths. The channel

matrix is described by the following equation,

$$H(t, f) = \sum_{k=1}^K \sum_{l=1}^{L_k} g_{kl}(t, f) \mathbf{u}_{rx}(\theta_{kl}^{rx}, \phi_{kl}^{rx}) \mathbf{u}_{tx}^*(\theta_{kl}^{tx}, \phi_{kl}^{tx}) \quad (2)$$

where, K is the number of clusters, L_k the number of subpaths in cluster k , $g_{kl}(t, f)$ the small-scale fading over frequency and time, $\mathbf{u}_{rx}(\cdot)$ is the spatial signature of the receiver and $\mathbf{u}_{tx}(\cdot)$ the spatial signature of the transmitter.

As given in [2], the small-scale fading is generated by,

$$g_{kl}(t, f) = \sqrt{P_{kl}} e^{2\pi i f_d \cos(\omega_{kl})t - 2\pi i \tau_{kl} f} \quad (3)$$

where P_{kl} is the power of subpath kl , f_d is the maximum Doppler shift, ω_{kl} is the angle between the subpath kl and the direction of motion of the receiver, τ_{kl} gives the delay spread and f is the carrier frequency.

Beamforming. Two methods are implemented in the **MmWaveBeamforming** class to compute beamforming vectors, which are termed the *power method* and *swipe sector method*. For the power method, we assume that the BS knows the channel matrices and can compute the largest singular value and singular vector associated with the strongest path. The swipe sector method implements a basic synchronization technique where the cell is divided into fixed sectors. The BS and UE scan all sectors (i.e., they perform beam switching) and select the beam with maximum gain based on the pre-stored beamforming vectors and does not require the channel state information to be known, but takes additional time to scan the cell. We provide this basic code as a basis for implementing more advanced cell search and synchronization protocols.

Channel Configuration. For both methods, the channel matrices and optimal beamforming vectors are pre-generated in MATLAB[®] to reduce the computational overhead in ns-3. At the beginning of each simulation we load 100 instances of the spatial signature matrices, along with the beamforming vectors.

In order to simulate realistic channels with large-scale fading, the channel matrices are updated periodically for NLoS channels but remain constant for LoS links as they are inherently more stable. Currently, no results are available for modeling how the large-scale statistics of the mmWave chan-

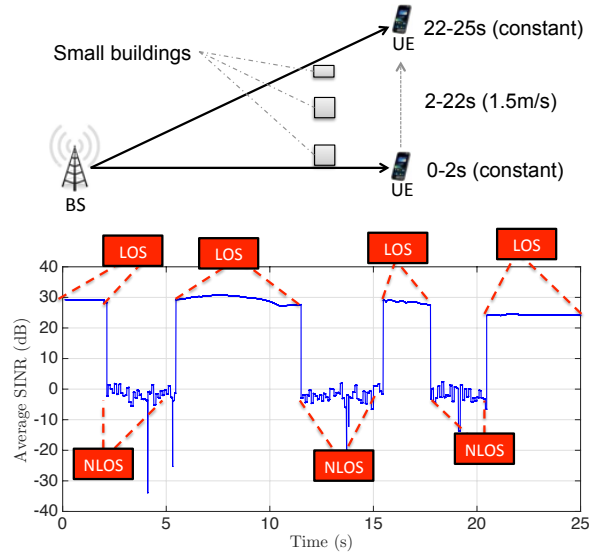


Figure 3: Average SINR plot for simulated route.

nel change over time for a mobile user. We therefore implement a form of large-scale *block fading*, where we update the channel by randomly selecting one of the 100 channel matrices/beamforming vector combinations after some interval. The large-scale parameters of the channel are thus independent in each interval. The update time can be some fixed interval specified by the `LongTermUpdatePeriod` attribute of the `MmWaveBeamforming` class. We also provide the option to update after a time drawn from an exponentially-distributed random variable (i.e., a Poisson process) with the mean also defined by the update period attribute. It should be noted that the accuracy of this method is not verified at this time.

The small-scale fading is calculated at every transmission based on Equation 3 where we obtain the speed of the user directly from the mobility model. The remaining parameters depending on the environment are assumed to be constant over the entire simulation time.

From Figure 3 we observe the average SINR trend obtained in the scenario where 3 buildings are distributed between BS and UE. The number of antennas at the BS and UE is 64 and 16, respectively. The user starts moving at a speed of 1.5 m/s 2 seconds after the start of the simulation and stops after 20 seconds. While the user is static (0-2s and 22-25s), as expected, the SINR is constant over time. However, when the user is in motion the Doppler effect causes the SINR to vary over time. The sudden SINR jumps indicate channel state switches, and as mentioned above, the channel matrices are updated every 100ms for the NLoS channel and remain unchanged for LoS transmissions.

3.3.2 Ray Tracing-Generated Model

In order to better characterize the time dynamics of the mmWave channel, we have added a ray tracing-generated channel model that computes the channel matrices in ns-3. The input is ray tracing data from real-world measurements, although such traces can also be generated by ray-tracer software.³ This channel model offers more flexibility to customize parameters, such as transmit and receiver antenna elements. Figure 4 shows the average SINR generated in ns-

³The ray tracing data is provided by Communication Systems and Networks Group, University of Bristol, UK.

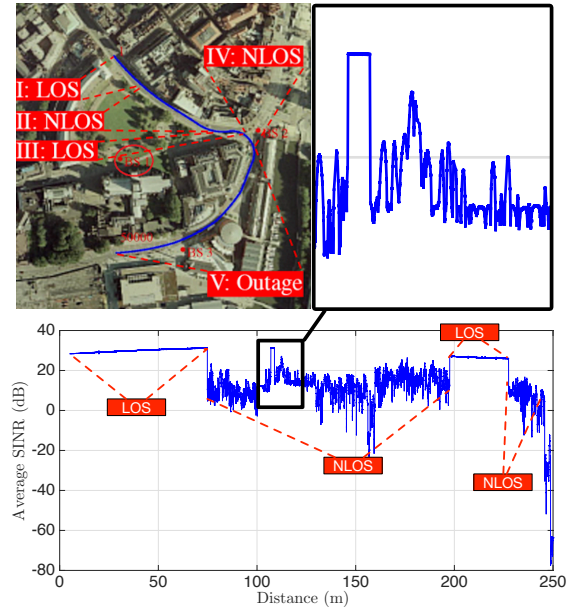


Figure 4: Average SINR plot for raytracing route.

3 by measuring a given ray path, with 64 transmit and 16 receive antennas. Propagation loss and channel matrices are computed according to Equation 2, where parameters are obtained from the ray tracing data containing 5000 samples within a 500 meter-long route. Each sample includes the following fields,

- Number of paths
- Propagation loss per path
- Delay per path
- Angle of arrival (elevation and azimuth plane) per path
- Angle of departure (elevation and azimuth plane) per path

As the user moves, the channel matrices are updated accordingly. For example, if the current location of the user is 10.1 meters from the BS, channel matrices are computed using the data corresponding to this distance.⁴ The beamforming vectors are generated using the power method as discussed earlier.

Figure 4 plots the average SINR indicating both LoS intervals and NLoS channel states. The SINR has a sudden change when channel state switches. We note that the SINR curve within LoS matches our simulation generated model, but for NLoS the ray tracing based model introduces more randomness variation.

3.3.3 Interference

Albeit potentially less significant for directional mmWave signals, which are generally assumed to be power-limited, there are still some cases where interference is non-negligible. For instance, although intra-cell interference (i.e. from devices of the same cell) can be neglected in TDMA or FDMA-mode operation, it does need to be explicitly calculated in the case of SDMA/Multi-User MIMO, where users are multiplexed in the spatial dimension but operate in the same time-frequency resources. Therefore, we propose an interference computation scheme that takes into account the beamforming vectors associated with each link.

⁴The minimum resolution is 10 cm.

As an example, we compute the SINR between nodes BS_1 and UE_1 in the presence of an interferer, UE_2 . To do so, we first need to obtain the channel gains associated with both the desired and interfering signals. Following Equation 2, we get

$$\begin{aligned} G_{11} &= |\mathbf{w}_{rx11}^* H(t, f)_{11} \mathbf{w}_{tx11}|^2, \\ G_{21} &= |\mathbf{w}_{rx11}^* H(t, f)_{21} \mathbf{w}_{tx22}|^2. \end{aligned} \quad (4)$$

We can now compute the SINR:

$$SINR_{11} = \frac{\frac{P_{Tx,11}}{PL_{11}} G_{11}}{\frac{P_{Tx,22}}{PL_{21}} G_{21} + BW \times N_0}, \quad (5)$$

where $P_{Tx,11}$ is the transmit power of BS_1 , PL_{11} is the pathloss between BS_1 and UE_1 , and $BW \times N_0$ is the thermal noise.

4. MAC LAYER

The high-level structure and functions of the mmWave MAC layer are now introduced. In particular, the two scheduler classes, multi-process stop-and-wait Hybrid ARQ (for both the downlink and uplink), along with some minor changes that have been made to the LENA module AMC and MI error model classes, are described in the following sections.

4.1 MAC Scheduling

We now present the implementation of two scheduler classes, which are based on a variable-length or *flexible* TTI, Time-Division Multiple Access (TDMA) scheme.

TDMA is widely assumed to be the de-facto scheme for mmWave access because of the dependence on analog beamforming, where the transmitter and receiver align their antenna arrays to maximize gain in specific direction (instead with a wide angular spread or omni-directionally, like conventional antennas). Many early designs and prototypes have been TDMA-based [6, 7], with others incorporating SDMA for the control channel only [8]. While SDMA or FDMA schemes (like in LTE) are possible with *digital beamforming*, which would allow the base station to transmit and receive in multiple directions within the same time slot, they may not be practical for mmWave systems due to high power consumption from requiring Analog-to-Digital Converters (ADCs) on each antenna element [9].

Furthermore, one of the foremost considerations driving innovation for the 5G MAC layer is latency. Specifically, the Key Performance Indicator (KPI) of 1 ms over-the-air latency has been proposed by such standards bodies as the ITU, as well as recent studies such as those carried out under the METIS 2020 project [11], as one of the core 5G requirements. However, a well-known drawback of TDMA is that fixed slot lengths or TTIs can result in poor resource utilization and latency, which can become particularly severe in scenarios where many intermittent, small packets must be transmitted to/received from many devices.

Based on these considerations, variable TTI-based TDMA frame structures and MAC schemes have been proposed in [8, 9, 12]. This approach allows for slot sizes that can vary according to the length of the packet or Transport Block (TB) to be transmitted and are well-suited for diverse traffic since they allow both bursty or intermittent traffic with small packets as well as high-throughput data like streaming and file transfers to be scheduled efficiently and without significant under-utilization.

4.1.1 Round-Robin Scheduler

The `MmWaveFlexTtiMacScheduler` class is the default scheduler for the mmWave module. It implements a variable TTI scheme previously described in Section 3 and assigns OFDM symbols to user flows in Round-Robin (RR) order. Upon being triggered by a subframe indication, any HARQ retransmissions are automatically scheduled using whatever OFDM symbols are available. While the slot allocated for a retransmission does not need to start at the same symbol index as the previous transmission of the same TB, they do need the same number of contiguous symbols and Modulation and Coding Scheme (MCS), since an adaptive HARQ scheme has not yet been implemented.

Before scheduling new data, Buffer Status Report (BSR) and Channel Quality Indication (CQI) messages are first processed. The MCS is then computed by the AMC model for each user based on the CQIs for the downlink or SINR measurements for the uplink data channel. The MCS, along with the buffer length of each user, are used to compute the minimum symbols required to schedule the data in the user's RLC buffers.

To assign symbols to users, the total number of users with active flows is calculated. Then the total available data symbols in the subframe are divided evenly among users. If a user requires fewer symbols to transmit its entire buffer, then the remaining symbols are distributed among the other active users.

One also has the option set a fixed number of symbols per slot by enabling *fixed TTI* mode. The one advantage of this scheme, as discussed in [9], is that the control overhead for DCI messages is lower. However, utilization and latency are likely to suffer.

4.1.2 Max-Weight Scheduler

The `MmWaveFlexTtiMaxWeightMacScheduler` class is similar to the RR scheduler but is intended to provide various priority queue policies. Currently only an Earliest Deadline First (EDF) policy is implemented, which weights flows by their relative deadlines for packet delivery, which are determined by the delay budget of the QoS Class Indicator (QCI) configured by the RRC layer. We have used this EDF scheduler to evaluate the delay performance of various radio frame configurations, although the results of this analysis are outside the scope of this paper. Other weight-based disciplines, such as Proportional Fair (PF) scheduling, will be added in future versions.

4.2 Adaptive Modulation and Coding

The `MmWaveAmc` class recycles most of the code from the corresponding LENA module class. Some minor modifications and additional methods were necessary to accommodate the dynamic TDMA MAC scheme and frame structure. For instance, the `GetTbSizeFromMcsSymbols()` and `GetNumSymbolsFromTbsMcs()` methods are used by the scheduler to compute the TB size from the number of symbols for a given MCS value, and visa-versa. Also the `CreateCqiFeedbackWbTdma()` method is added to generate wideband CQI reports for variable-TTI slots.

Figure 5 shows the results of the test case provided in *mmwave-amc-test.cc*. This simulation serves to demonstrate the performance of the AMC and CQI feedback mechanisms for a single user in the uplink (although a multi-user scenario could easily be configured, as well). The default PHY/MAC

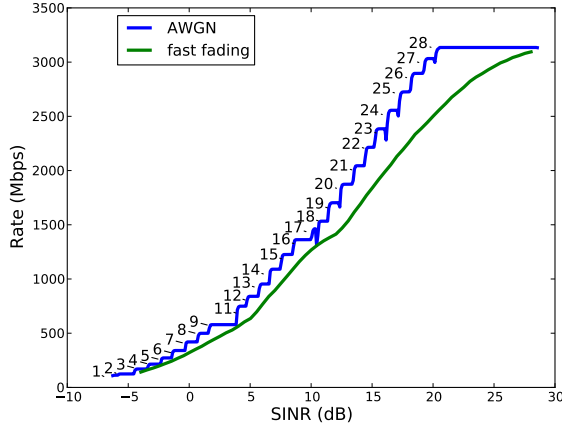


Figure 5: Rate and MCS vs. SINR for single user under AWGN and fast-fading mmWave channels

parameters in Table 1 are used along with the default scheduler and default parameters for the statistical path loss, fading and beamforming models (i.e. `MmWavePropagationLoss-Model` and `MmWaveBeamforming`).

We compute the rate versus the average SINR over a period of 12 seconds (long enough to the small-scale fading to average out), after which we artificially increase the path loss while keeping the UE position fixed. The average PHY-layer rate is then computed as the average sum size of successfully-decoded TBs per second. As the SINR decreases, the MAC will select a lower MCS level to encode the data. The test is performed for the AWGN case as well as for small-scale fading. Although we the UE position relative to the base station is constant, we can generate time-varying multi-path fading through the `MmWaveBeamforming` class by setting a fixed speed of 1.5 m/s to artificially generate Doppler, which is a standard technique for such analysis. Also we assume the long-term channel parameters do not change for the duration of the simulation.

If this plot is compared to the one generated from a similar test in Figure 3.1 of the LENA documentation [5], we notice that the AWGN curve from the mmWave test is shifted by approximately 5 dB to the left, indicating that the LENA version is transitioning to a lower MCS at a much higher SINR. This is because the LENA test is using the more conservative average SINR-based CQI mapping. In our test, we use the Mutual Information-Based Effective SINR (MIESM) scheme with a target maximum TB error of 10% in order to maximize the rate for a given SINR.

4.3 Hybrid ARQ Retransmission

Full support for HARQ with soft combining is now included in the mmWave module. The `MmWaveHarqPhy` class along with the functionality within the scheduler are based heavily on the LENA module code. However, multiple HARQ processes per user in the uplink are now possible. The number of processes can also be configured through the `NumHarqProcesses` attribute in `MmWavePhyMacCommon`. Additional modifications were needed to support larger codeword sizes in both the HARQ PHY methods as well as the error model.

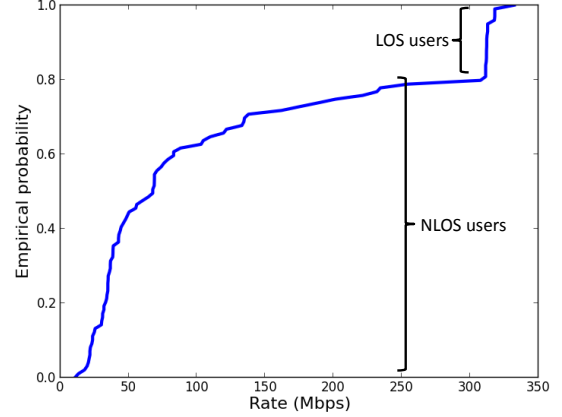


Figure 6: Empirical CDF of downlink user rates for 10 users with RR scheduling.

5. EXAMPLE SIMULATIONS

We now present some example simulations to show the utility of the framework for analysis of novel mmWave protocols and testing higher-layer network protocols, such as TCP, over 5G mmWave networks. The simulations in this section are all configured with basic PHY and MAC parameters in Table 1, with other notable parameters given in the sequel.

5.1 Multi-User Throughput Simulation

The purpose of this experiment, which one can reproduce by running the `mmwave-tdma` example, is to simulate the downlink throughput of 10 UEs in a 1 GHz mmWave cell under the variable TTI/TDMA MAC scheme and round-robin scheduling policy. UEs are placed at uniformly random distances between 20 and 200 meters from a single eNodeB. As explained in Section 4.2, users are stationary but are modeled as having a constant speed of 1.5 m/s and are thus subject to small-scale fading. The long-term channel parameters are updated based on the exponentially-distributed update time with a mean of 100 ms (see Section 3.3). Rates are computed from the average size of RLC PDUs delivered to each UE and therefore reflect the performance of the stack up to and including the RLC layer. We assume full-buffer traffic.

The simulation is performed for 10 runs or *drops* of the 10 UEs, where for each drop they are placed at different distances and assigned different channel matrices. The average system throughput at the RLC layer for this scenario over all drops is found to be about 1.2 Gb/s. We observe in the plot of the empirical distribution function in Figure 6 how UEs with LoS links all have roughly the same average rates around 325 Mb/s. Also a significant number of NLoS users achieve rates over 100 Mb/s, and even the worst 5% of users at the cell edge can get between 10-20 Mb/s.

5.2 TCP Performance over mmWave

Here run the `mmwave-tcp-building` example to analyze the performance of TCP flows over a mmWave link. TCP data packets are sent from a remote host to the UE at a rate of 1 Gbps. The New Reno algorithm is used for this experiment and the delay for the point-to-point link between the remote host and PDN-Gateway (PGW), as well as the PGW to the

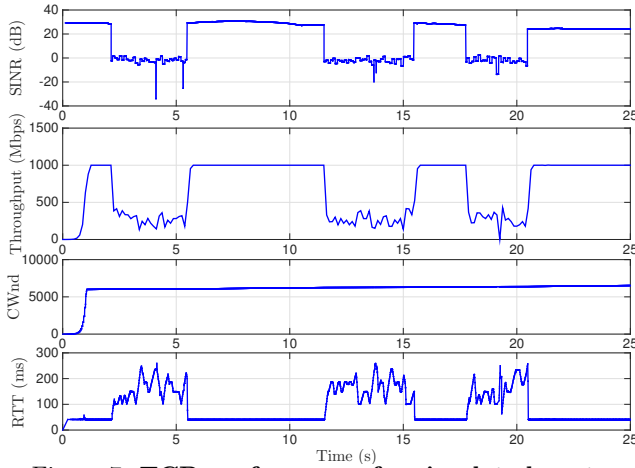


Figure 7: TCP performance for simulated route.

BS, is set at 10 ms. Thus, the contribution to the total Round Trip Time (RTT) from the core network should be around 40 ms and any additional latency is thanks to the radio link, which, under stable queue conditions, is observed to be less than 10 ms. The size of the RLC-AM buffer is adjusted to 10 Megabytes to avoid overflow. The TCP buffer size is set to 5 Megabytes and the slow start threshold is 6000.

Figure 7 plots the SINR, transport layer throughput, congestion window size (CWnd) and the RTT. As shown, the transport layer throughput matches the sending rate for the LoS channel, but is reduced when the channel is in the NLoS state. This is attributed to the MAC-layer AMC model adapting to the change in capacity. From the congestion window plot we see that there is no TCP timeout or retransmission since the packet loss events are handled by lower layer retransmissions, i.e. MAC layer HARQ and RLC ARQ. Moreover, we see the RTT for LoS channel around the baseline 40 ms but goes above 150 ms for the NLoS case. It is clear that decreased channel capacity and more frequent RLC retransmission events causes the RLC buffer to become backlogged, which explains the increase in RTT. This result suggests the need for more a more advanced congestion control mechanism, perhaps aided by feedback or control from lower layers, to prevent large spikes in latency under rapid channel fluctuations.

6. CONCLUSIONS & FUTURE WORK

In this paper, the current state of the ns-3 framework for simulation of mmWave cellular systems has been presented. The code, which is publicly available at GitHub [13], is highly modular and customizable to facilitate researchers to experiment with novel 5G protocols. The code includes implementations of a mmWave eNodeB and User Equipment stack, including the MAC layer, PHY layer and channel models. Some example simulations have been given, which show how the framework may be used for analysis of custom mmWave PHY/MAC protocols as well as higher-layer network protocols over a mmWave stack and channel.

As part of our future work, we have targeted several new features for channel modeling including a more accurate model for large-scale fading for mobile users as well as channel matrix generation and beamforming computation within ns-3 to support experimentation with adaptive beamforming

algorithms. Future enhancements to the MAC layer include support for other multiple access schemes, relay devices, and additional scheduling algorithms.

7. REFERENCES

- [1] S. Rangan, T. S. Rappaport, and E. Erkip, "Millimeter-wave cellular wireless networks: Potentials and challenges," *Proc. IEEE*, vol. 102, no. 3, pp. 366–385, Mar. 2014.
- [2] M. Akdeniz, Y. Liu, M. Samimi, S. Sun, S. Rangan, T. Rappaport, and E. Erkip, "Millimeter wave channel modeling and cellular capacity evaluation," *IEEE J. Sel. Areas Commun.*, vol. 32, no. 6, pp. 1164–1179, June 2014.
- [3] "ns3 Network Simulator," Available at <http://www.nsam.org>, Feb. 2012.
- [4] M. Mezzavilla, S. Dutta, M. Zhang, M. R. Akdeniz, and S. Rangan, "5G mmwave module for the ns-3 network simulator," in *Proceedings of the 18th ACM International Conference on Modeling, Analysis and Simulation of Wireless and Mobile Systems (MSWiM '15)*.
- [5] C. T. de Telecomunicacions de Catalunya (CTTC), "The LENA ns-3 LTE Module Documentation," Available at [http://iptechwiki.cttc.es/LTE-EPC_Network_Simulator_\(LENA\)](http://iptechwiki.cttc.es/LTE-EPC_Network_Simulator_(LENA)), Jan.
- [6] Z. Pi and F. Khan, "System design and network architecture for a millimeter-wave mobile broadband MMB system," in *Proc. IEEE Sarnoff Symposium*, May 2011.
- [7] A. Ghosh, T. A. Thomasa, M. C. Cudak, R. Ratasuk, P. Moorut, F. W. Vook, T. S. Rappaport, J. G. R. MacCartney, S. Sun, and S. Nie, "Millimeter-wave enhanced local area systems: A high-data-rate approach for future wireless networks," *IEEE J. Sel. Areas in Comm.*, vol. 32, no. 6, pp. 1152–1163, June 2014.
- [8] T. Levanen, J. Pirskanen, and M. Valkama, "Radio interface design for ultra-low latency millimeter-wave communications in 5G era," in *Proc. IEEE Globecom Workshops (Gc Wkshps)*, Dec. 2014, pp. 1420–1426.
- [9] S. Dutta, M. Mezzavilla, R. Ford, M. Zhang, S. Rangan, and M. Zorzi, "Frame structure design and analysis for millimeter wave cellular systems," in *arXiv:1512.05691 [cs.NI]*, Dec. 2015.
- [10] "Winprop software," Available at <http://www.awe-communications.com/Products/>.
- [11] P. Popovsk, V. Brau, H.-P. Mayer, P. Fertl, Z. Ren, D. Gonzales-Serrano, E. G. Ström, T. Svensson, H. Taoka, P. Agyapong *et al.*, "EU FP7 INFOS-ICT-317669 METIS, D1. 1 scenarios, requirements and KPIs for 5G mobile and wireless system," 2013.
- [12] P. Kela, M. Costa, J. Salmi, K. Leppanen, J. Turkka, T. Hiltunen, and M. Hronec, "A novel radio frame structure for 5G dense outdoor radio access networks," in *Proc. IEEE 81st Vehicular Technology Conference (VTC Spring)*, May 2015, pp. 1–6.
- [13] "ns-3 module for simulating mmwave-based cellular systems," Available at <https://github.com/mmezzavilla/ns3-mmwave>.